Prenatal lipopolysaccharide exposure programs cardiac fibrosis via dysregulating of connexin 43 in offspring rats

YAN WEN[1,2], YAO YUAN[1], HAIGANG ZHANG[1] and YA LIU[1]

[1]Department of Pharmacology, College of Pharmacy, Army Medical University, Chongqing 400038, P.R. China;
[2]Department of General Surgery, The First Affiliated Hospital of Army Medical University, Chongqing 400038, P.R. China

Received August 14, 2025; Accepted January 23, 2026

DOI: 10.3892/mmr.2026.13830

Abstract. The present study investigated the role of connexin 43 (Cx43) in mediating prenatal inflammation-induced cardiac fibrosis in offspring, specifically exploring its dynamic regulation with autophagy and DNA methylation pathways. Pregnant Sprague-Dawley rats received intraperitoneal injections of saline (control) or lipopolysaccharide (LPS, 0.79 mg/kg) on gestational days 8, 10 and 12. Offspring were sacrificed at 8 and 16 weeks postpartum. Myocardial tissues were subjected to histopathological examination and molecular analysis. Prenatal LPS exposure consistently induced significant cardiac fibrosis in the offspring. Reverse transcription-quantitative PCR revealed that mRNA levels of *Cx43*, *LC3* and DNA methyltransferase 1 (*DNMT1*) were markedly reduced at 8 weeks; however, they were elevated above control levels at 16 weeks. Western blotting revealed persistent suppression of Cx43 protein expression at both ages, whereas the LC3-II/I ratio and DNMT1 protein levels paralleled the biphasic mRNA trends. *In vitro* experiments using neonatal rat cardiac fibroblasts treated with LPS (10 μg/ml, 24 h) confirmed Cx43 and LC3 downregulation and DNMT1 upregulation. Targeted pharmacological interventions were used to clarify these regulatory relationships. Cotreatment with the Cx43 gap junction inhibitor carbenoxolone (400 μM) and LPS further suppressed Cx43, LC3 and DNMT1 expression. However, cotreatment with the Cx43 agonist all-trans retinoic acid (10 μM) attenuated LPS-induced DNMT1 upregulation and LC3-II/I ratio suppression. These findings demonstrate that the functional state of Cx43 critically links fetal inflammatory insults to postnatal cardiac fibrogenesis by dynamically regulating interconnected autophagy and DNA methylation, establishing Cx43 as an upstream regulatory node in this pathogenic network.

Correspondence to: Dr Ya Liu, Department of Pharmacology, College of Pharmacy, Army Medical University, 30 Gaotanyan Main Street, Shapingba, Chongqing 400038, P.R. China
Email: liuya0321@tmmu.edu.cn

Key words: intrauterine inflammation, connexin 43, cardiac fibrosis, autophagy, DNA methylation

Introduction

Cardiac fibrosis is characterized by excessive deposition of extracellular matrix (ECM) proteins, representing a common pathological endpoint in nearly all forms of heart disease, including myocardial infarction, aortic stenosis, hypertrophic cardiomyopathy and diabetic cardiomyopathy. This maladaptive remodeling process directly contributes to heart failure development and exacerbates adverse outcomes in established patients with heart failure (1). Cardiac fibroblasts (CFs) are the second most abundant cell population in the heart after cardiomyocytes and are pivotal for fibrogenesis through their exceptional plasticity and secretory capacity. These cells dynamically transition between differentiation states in response to cardiac injury, aging, genetic predisposition and environmental factors, actively secreting ECM structural proteins, proteolytic enzymes, growth factors and cytokines that collectively drive pathological collagen deposition (1). Despite significant advances in identifying fibrogenic signaling pathways, the absence of specific anti-fibrotic therapies highlights the urgent need for novel mechanistic insights and therapeutic targets.

The Developmental Origins of Health and Disease (DOHaD), initially proposed by Barker, has gained significant scientific recognition (2). Maternal inflammatory conditions, including periodontitis, urethritis and influenza, are common challenges during gestation. This exposure creates an intrauterine environment characterized by elevated proinflammatory cytokines and associated mediators, potentially predisposing offspring to cardiovascular pathologies, including hypertension and cardiac hypertrophy. Our previous studies using lipopolysaccharides (LPS), a gram-negative bacterial cell wall component, in pregnant rodent models have provided supporting evidence (3-5). In these distinctive models, offspring rats born to LPS-exposed dams revealed moderate elevation in collagen synthesis without apparent cardiac dysfunction at 6 weeks of age, yet developed significant left ventricular (LV) hypertrophy by 8 months (4). Notably, prenatal LPS-exposed mice demonstrated exacerbated cardiac fibrosis responses to isoproterenol challenge as early as 4 weeks postnatal, despite baseline fibrosis levels remaining comparable between the exposed and control groups at this developmental stage (5). These observations highlight the need to study the molecular mechanisms underlying the developmental programming of cardiac vulnerability.

Dysregulation of intercellular communication is associated with the pathological changes of fibrosis (6). Gap junctions (GJs), composed of connexin proteins (Cxs), particularly Cx43 in cardiac tissue, facilitate key cardiomyocyte-fibroblast crosstalk through ion exchange and metabolite transfer (7,8). Cx43-mediated communication modulates fibroblast activation, phenotypic switching and pathological coupling with cardiomyocytes, thereby covering all the key processes in fibrogenesis (7,8). Notably, the autophagy pathway is an essential quality control mechanism for cellular components, including connexins and has emerged as a potential regulator of fibrotic progression (9,10). The short half-life of Cx43 makes its turnover particularly dependent on autophagic degradation, creating a potential mechanistic association between these pathways in cardiac pathology (10).

Epigenetic dysregulation, particularly DNA methylation alterations, may be a critical mechanism underlying the developmental programming of fibrosis. Our previous study established that prenatal LPS exposure induces hypertension in offspring associated with renal and vascular methylation changes (11,12). This, coupled with emerging evidence connecting DNA methylation to both autophagy regulation and Cx43 dysfunction, prompted us to hypothesize that methylation-involved interactions between Cx43 and autophagy drive the developmental programming of cardiac fibrosis. Therefore, the present study systematically investigated these mechanistic relationships in a well-characterized rat model of prenatal LPS exposure, aiming to identify novel therapeutic targets for preventing maternal inflammation-primed cardiac fibrosis.

Materials and methods

Animal treatment. A total of 16 female nulliparous, pregnant Sprague-Dawley rats (age, 10 weeks; weight, 180-220 g) were obtained from the Experimental Animal Center of Army Medical University. Animals were individually housed in a controlled environment at a constant temperature (24˚C), relative humidity of 50±10%, under a 12-h light/dark cycle with *ad libitum* access to standard laboratory chow and water. Following a 5-day acclimation period, pregnant dams were randomly allocated to the control (n=8) or LPS (n=8) treatment groups. Subjects received intraperitoneal injections of either 0.5 ml saline (control) or 0.79 mg/kg LPS (MilliporeSigma) on gestational days 8, 10 and 12, which is a critical window for embryonic cardiogenesis. Postpartum litter parameters, including size and individual pup weights, were recorded. To standardize nutritional availability, litters were culled to eight neonates/dam until weaning at postnatal week 4. Post-weaning offspring were group-housed by sex (4-5 animals/cage) and given continuous access to food and water, under the same controlled environmental conditions as those for the pregnant rats. Body weights were monitored weekly from birth through the study period. At 8 and 16 weeks of age, male offspring were randomly selected for terminal procedures. After being deeply anesthetized with sodium pentobarbital (50 mg/kg, i.p.), animals were sacrificed by exsanguination via cardiac puncture while under deep anesthesia. Mortality was confirmed by the cessation of respiration, loss of corneal reflex and direct visual confirmation of cardiac arrest via thoracotomy prior to tissue harvest (13). Blood and cardiac tissue samples were then collected immediately for subsequent analyses.

Heart weight index and LV mass index. The heart was perfused with ice-cold physiological saline to remove any residual blood. Excess pericardial tissue and the surrounding vasculature were carefully dissected away, followed by moisture removal through gentle blotting with filter paper. The total cardiac mass was recorded using an analytical balance. The LV myocardium was surgically isolated from the cardiac base along the interventricular groove. Morphometric indices were subsequently calculated as the ratio of total heart weight (HW) or LV weight (LVW) to body weight (BW), expressed as HW/BW and LVW/BW, respectively.

Measurement of B-type Natriuretic Peptide (BNP) and angiotensin II (Ang II) levels. Following a 30-min clotting period at room temperature, whole blood samples were centrifuged at 3,000 x g for 15 min to isolate the serum. LV tissue specimens were immediately homogenized in ice-cold phosphate-buffered saline (PBS; 50 mg tissue/0.5 ml) containing 1% nonidet-P40 (Shanghai Biyuntian Biotechnology Co., Ltd.) and a complete protease inhibitor cocktail using a mechanical tissue homogenizer. The resulting homogenates were centrifugated at 12,000 x g for 10 min at 4˚C in a refrigerated centrifuge to obtain clarified supernatants. Serum concentrations of N-terminal pro-BNP (NT-proBNP; cat. no. E-EL-R3023) and Ang II, along with myocardial tissue levels of Ang II (cat. no. E-EL-R1430c), were quantified using commercial ELISA kits (Elabscience Biotechnology Co., Ltd.) following manufacturer protocols. All assays included appropriate quality controls and standard curve validation.

Histological analysis. All procedures were performed at room temperature. LV tissues were immersion-fixed in 4% paraformaldehyde for 24-48 h, before paraffin embedding. Serial sections (4 μm) were prepared using a rotary microtome. For basic histoarchitecture evaluation, the sections were stained with hematoxylin and eosin (H&E; hematoxylin staining for 5 min, eosin staining for 2 min). Collagen fiber visualization was achieved using Masson's trichrome staining performed following manufacturer specifications (Beijing Solarbio Science & Technology Co., Ltd.). After overnight incubation in potassium dichromate solution, the sections underwent ferric hematoxylin staining for 6 min, followed by acid fuchsin staining for 8 min, phosphomolybdic acid treatment for 2 min, and aniline blue staining for 2 min. Prior to sectioning, the samples subjected to sequential dehydration through a graded ethanol series (70-100%), xylene clearing and paraffin infiltration. The stained sections were imaged using bright-field microscopy (Nikon Eclipse E100; Nikon Corporation). Quantitative assessment of myocardial fibrosis was performed by calculating the collagen volume fraction (CVF) through systematic random sampling of five non-overlapping high-power fields (magnification, x400) per section. CVF was determined as the percentage ratio of the aniline blue-stained collagen area to the total myocardial area using the image analysis software (version 6.0; Media Cybernetics, Inc.).

Immunofluorescence staining. LV tissues embedded in OCT compound (OriGene Technologies, Inc.) were cryosectioned into four sequential 10-μm-thick sections using a cryostat (Leica CM1950) and mounted on poly-L-lysine-coated slides. For immunofluorescence detection, the slides were first blocked with 10% normal goat serum (Life Technologies; cat. no. 50062Z) in PBS containing 0.2% Tween-20 for 1 h at room temperature. Sections were incubated overnight at 4˚C with rabbit polyclonal anti-α-smooth muscle actin (α-SMA) antibody (1:400 dilution; Abcam. cat. no. ab124964) in a humidified chamber. After three PBS washes (5 min each), the slides were incubated with Cy3-conjugated goat anti-rabbit IgG secondary antibody (1:400 dilution; Invitrogen; Thermo Fisher Scientific, Inc. A10520) for 1 h at room temperature, protected from light. Negative control slides were processed identically, except for primary antibody omission. Fluorescent images were captured using a laser-scanning confocal microscope (Olympus FV3000; Olympus Corporation) with excitation/emission wavelengths of 550/570 nm for Cy3 detection.

Neonatal rat cardiac fibroblasts Isolation and treatment. CFs were isolated from neonatal Sprague-Dawley rats (1-3 days postnatal) using established enzymatic digestion protocols. Prior to sacrifice, neonatal pups were anesthetized by hypothermia, which involved placement on a sterile ice-cold surface for 3-5 min until unresponsive to a toe pinch, ensuring a surgical plane of anesthesia (14). Following confirmation of deep anesthesia, the pups were sacrificed by rapid decapitation and immediately surface-sterilized through two sequential 10-sec immersions in 75% ethanol. Ventricular tissue was dissected free from atria, minced into 1 mm^3 fragments and washed twice with Dulbecco's modified Eagle's Medium (DMEM). Tissue fragments underwent five sequential digestions (5-min intervals) in an enzymatic solution containing 0.5% collagenase type I (Worthington Biochemical Corporation) and 0.05% trypsin (Gibco; Thermo Fisher Scientific, Inc.) and maintained at 37˚C in an oscillating water bath. After centrifugation at 300 x g for 5 min, cell pellets were resuspended in complete culture medium [DMEM supplemented with 10% fetal bovine serum (FBS; HyClone™; Cytiva] and incubated under standard culture conditions (37˚C and 5% CO_2). CFs were purified through differential adhesion by discarding cardiomyocyte-containing supernatant after 2 h of initial plating. Cells from third-passage cultures were used for experiments following serum starvation (24 h in DMEM without FBS). For the subsequent treatments, the cells were divided into four groups: A control group receiving culture media alone; an LPS group treated with 10 μg/ml LPS for 24 h; an LPS + carbenoxolone (CBX) group co-treated with 10 μg/ml LPS and 400 μM CBX (MilliporeSigma), a specific Cx43 gap junction inhibitor; an LPS + all-trans retinoic acid (ATRA) group co-treated with 10 μg/ml LPS and 10 μM ATRA (MilliporeSigma), a Cx43 agonist, for 24 h.

RNA preparation and reverse transcription-quantitative (RT-q) PCR. Total RNA was isolated from LV tissue and cells using the Total RNA Extraction kit (Tiangen Biotech, Co., Ltd.). RT was performed using GoScript™ RT System (Promega Corporation) according to the manufacturer's instructions. RT-qPCR was carried out using Bestar® SYBR Green qPCR Mastermix (DBI Biosciences. DBI-2043) according to the manufacturer's instructions. The primers were designed by Primer software (Premier 5.0; Premier Biosoft International) based on published nucleotide sequences for rat Cx43 (forward: 5'-GACTTCAGCCTCCAAGGAGTT-3'; reverse: 5'-ACCCCAAGCTGACTCAACAG3-3'), rat LC3 (forward: 5'-CCCTGCTAACCCCCAATGTT-3'; reverse: 5'-GGGACA TGACGACGTACACA'), rat DNMT1 (forward: 5'-GCTGT TCCTTGTAGGCGAGT-3'; reverse: 5'-GGGGACTCAAAC CTTGCGTA-3'), rat DNMT3A (forward: 5'-TGATGACGA GCCCGAGTATG-3'; reverse: 5'-GCCATC TCCGAACCA CATGA-3'), rat DNMT3B (forward: 5'-AATTACACGCAG GACGTGGT-3'; reverse: 5'-ACTGTTGCTGTT TCGGGT TC-3') and rat β-actin (forward: 5'-CCATTGAACACGGCA TTG-3'; reverse: 5'-TACGACCAGAGGCATACA-3'). The PCR cycling conditions were as follows: initial denaturation at 95˚C for 2 min, followed by 40 cycles of denaturation at 95˚C for 10 sec, annealing at 60˚C for 34 sec, and extension at 72˚C for 30 sec. Final melting curve analysis (65-95˚C, 0.5˚C increments, 5 sec per increment) was performed to confirm primer specificity. The relative expression levels of target genes were calculated using the $2^{-\Delta\Delta Cq}$ method (15), with β-actin serving as the internal reference gene. All experiments were independently replicated three times, with each replicate containing six technical replicates.

Western blotting. The LV samples and cells were processed and western blotting was conducted following the standard procedures. Briefly, tissue and cells were lysed in RIPA lysis buffer (Beyotime Institute of Biotechnology. P0013C) for 30 min on ice followed by centrifugation at 12,000 x g for 15 min at 4˚C to collect the supernatant. The enhanced BCA protein assay kit (Beyotime Biotechnology. cat. no. P0010) was used to determine the protein concentration. Equal amounts of protein (30 μg per lane) were separated by 10% sodium dodecyl sulfate-polyacrylamide gel electrophoresis (SDS-PAGE) and transferred onto 0.45 μm polyvinylidene fluoride (PVDF) membranes (Millipore. IPVH00010). The membranes were blocked with 5% non-fat dry milk (Santa Cruz Biotechnology. sc-2325) diluted in Tris-buffered saline with Tween-20 (TBST) at room temperature for 1 h, then incubated overnight at 4˚C with the following primary antibodies: anti-Cx43 (1:1,000; Abcam. ab11370), anti-microtubule-associated protein-1 light-chain (LC3; 1:1,000; Santa Cruz Biotechnology, Inc. sc-271625), anti-DNMT1 (1:500; Novus Biologicals, LLC; cat. no. NB100-56519), anti-DNMT3A (1:1,000; Novus Biologicals, LLC. NB120-13888), anti-DNMT3B (1:1,000; Novus Biologicals, LLC. NB300-516) and β-actin (1:1,000; Santa Cruz Biotechnology, Inc., USA. sc-47778) antibody were used. After three washes with TBST, the membranes were incubated with horseradish peroxidase (HRP)-conjugated goat anti-rabbit IgG (1:5,000; Zhongshan Golden Bridge Bio Co., Ltd. ZB-2301) or HRP-conjugated goat anti-mouse IgG (1:5,000; Invitrogen. A16084) at room temperature for 1 h. Protein bands were visualized using an Enhanced Chemiluminescence (ECL) Detection Kit (Thermo Fisher Scientific, Inc.) and imaged with a ChemiDoc XRS+ System

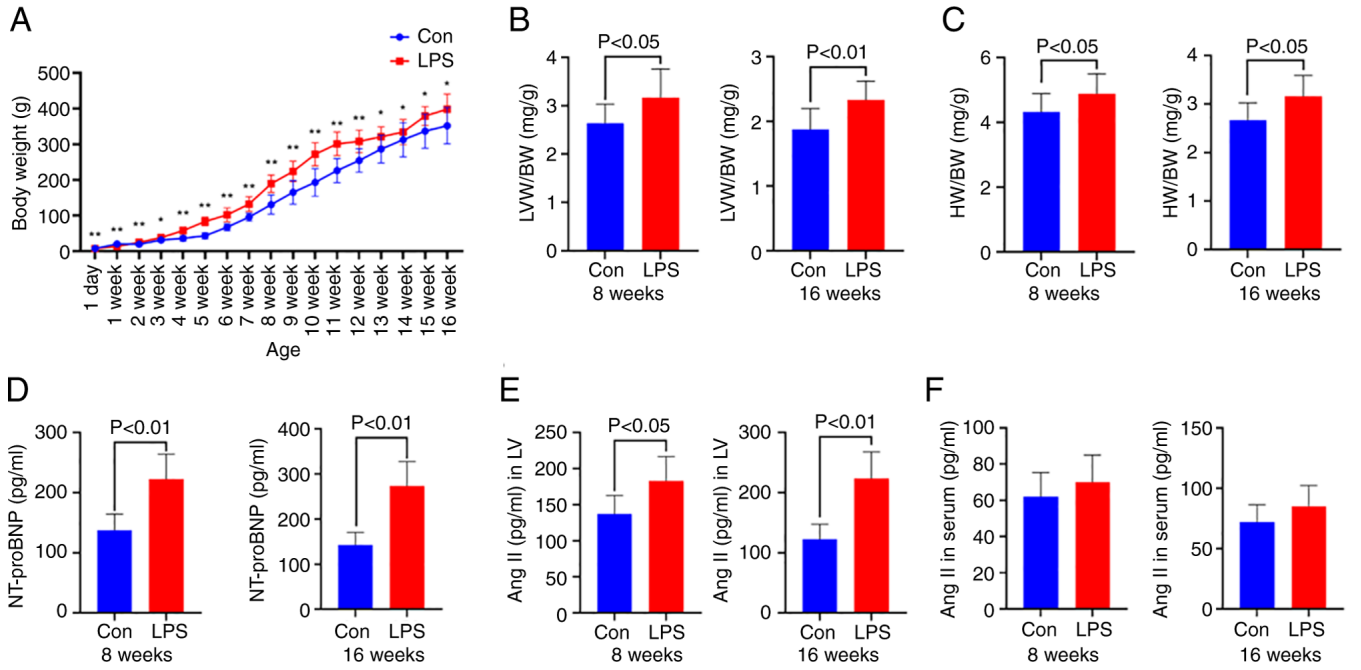

Figure 1. BW of offspring rats from 1-day to 16-week-old (A). Heart damages in offspring at the age of 8 and 16 weeks, including the ratios (B) LVW/BW, (C) HW/BW and (D) NT-proBNP level in serum. Concentration of Ang II in (E) left ventricle and (F) serum. Data are presented as mean ± SD. n=10 in each group (A-C) and n=7 in each group (D-F). *P<0.05, **P<0.01 vs Con. BW, body weight; HW, heart weight; LVW, left ventricular weight; NT-proBNP, N-terminal pro-brain natriuretic peptide; Ang II, angiotensin II; Con, control; LPS, lipopolysaccharide.

(Bio-Rad Laboratories, Inc.). Densitometric analysis of the bands was performed using Image J software (Version 1.50i, NIH) with β-actin as the internal loading control.

Statistical analysis. Data are presented as mean ± standard deviation (SD). Statistical analyses were performed with GraphPad Prism 9.0.0 software (Dotmatics). The Shapiro-Wilk test was adopted to evaluate the normality of data distribution, while Levene's test was used to examine the homogeneity of variance. An unpaired two-tailed Student's t-test was employed for comparisons between two independent groups. For multiple group comparisons, one-way ANOVA was conducted, followed by Dunnett's post hoc test. P<0.05 was considered to indicate a statistically significant difference.

Results

Cardiac impairment in prenatally LPS-exposed offspring rats. Newborns in the prenatal LPS exposure group exhibited markedly reduced BW compared with controls at both birth (P<0.01) and 1 week of age (P<0.01; Fig. 1). However, these LPS-exposed offspring demonstrated persistent weight gain acceleration from 2 weeks onward (P<0.05 or P<0.01), despite comparable daily feed intake between groups. Although postnatal catch-up growth can compensate for intrauterine growth restriction, excessive compensatory growth is strongly associated with adverse adult health outcomes (16). The findings revealed significant cardiac hypertrophy in LPS-exposed offspring, as evidenced by elevated LVW/BW and HW/BW ratios at both 8 (P<0.05) and 16 weeks (P<0.01). Concurrently, markedly increased circulating NT-proBNP levels, a ventricular stress biomarker reflecting volume overload and cardiac dysfunction were observed in 8-week (P<0.01) and 16-week-old (P<0.01) LPS-exposed offspring (17). While serum Ang II levels remained unaffected by prenatal LPS exposure, substantial increases in LV Ang II concentration were detected at 8 weeks (P<0.05) and 16 weeks (P<0.01). As the primary RAS agonist, Ang II mediates pressure overload-induced cardiac fibrosis and hypertrophy.

Heart histology alterations in prenatally LPS-exposed offspring rats. To assess cardiac morphological alterations induced by prenatal LPS exposure, myocardial architecture was examined through histological analysis using H&E and Masson staining. H&E staining revealed distinct pathological progression in LPS-exposed offspring. Control specimens exhibited preserved myocardial structure with tightly arranged cardiomyocytes. Conversely, 8-week-old LPS-exposed offspring demonstrated characteristic pathological features, including cellular edema, intercellular space widening, myocardial fiber disruption, focal necrosis and inflammatory cell infiltration. These pathological manifestations exhibited age-dependent progression, with 16-week-old LPS-exposed offspring exhibiting exacerbated myocardial degeneration characterized by extensive tissue damage and pronounced inflammatory infiltration (Fig. 2A). Masson staining revealed significant extracellular matrix remodeling in LPS-exposed groups. Collagen deposition (blue-stained fibers) within the LV interstitium was markedly increased compared with age-matched controls, with 8-week-old LPS-exposed offspring showing initial fibrosis that progressed substantially by 16 weeks of age. CVF quantitative analysis confirmed these observations, demonstrating statistically significant increases in the LPS-exposed groups at 8 weeks (P<0.01) and 16 weeks (P<0.01) compared with the controls (Fig. 2B).

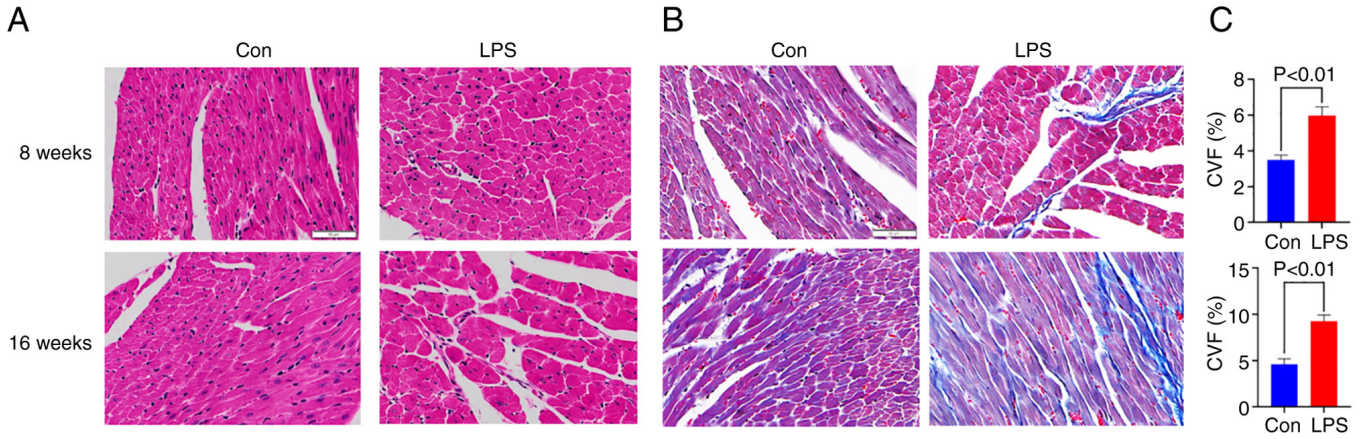

Figure 2. Histopathological observation of LV in 8- and 16-week-old offspring rats. (A) Hematoxylin and eosin staining. (B) Masson trichrome staining and (C) CVF. Data are presented as mean ± SD. n=6 in each group. LV, left ventricular; CVF, collagen volume fraction; Con, control; LPS, lipopolysaccharide.

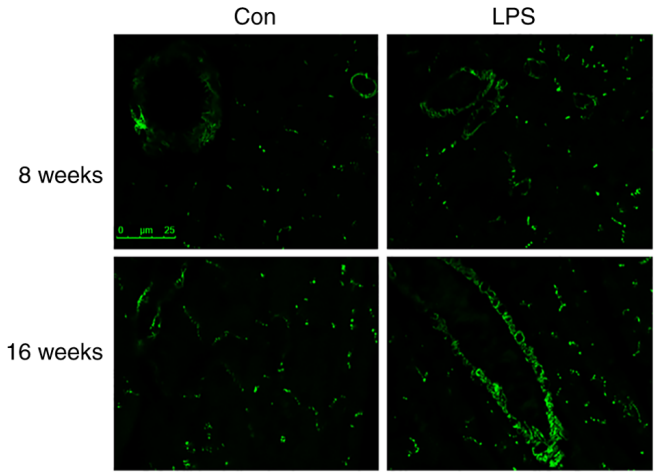

Figure 3. Immunolabeling of α-smooth muscle actin in the heart. Con, control; LPS, lipopolysaccharide.

α-SMA immunolabeling in LV samples. Complementing the histological findings, immunofluorescence staining was used to study CF differentiation into α-SMA-expressing myofibroblasts, a hallmark feature of fibrotic progression. Prenatal LPS exposure markedly activated this pathogenic transformation in the offspring myocardium. Compared with controls, 8-week-old LPS-exposed offspring exhibited a pronounced increase in α-SMA-positive cells in the LV, as evidenced by the elevated fluorescent signal intensity and cluster density. By 16 weeks of age, this activation progressed further, with LPS-exposed offspring demonstrating expansive α-SMA-positive bands and intensified fluorescence, indicative of advanced myofibroblast aggregation and sustained fibrosis (Fig. 3).

Cx43, LC3, DNMT1, DNMT3A and DNMT3B mRNA expressions in LV samples. RT-qPCR analysis revealed distinct age-dependent transcriptional alterations in the LPS-exposed offspring. Compared with controls, 8-week-old offspring with prenatal LPS exposure exhibited significant downregulation of *Cx43* (P<0.05), *LC3* (P<0.01) and *DNMT1* (P<0.01). However, these trends were reversed at 16 weeks of age, with elevated mRNA levels of *Cx43* (P<0.05), *LC3* (P<0.05) and *DNMT1* (P<0.01). Conversely, non-significant intergroup differences were observed in *DNMT3A* (P>0.05) or *DNMT3B* (P>0.05) expression at either developmental stage, suggesting isoform-specific regulatory mechanisms in DNA methylation (Fig. 4).

Cx43, LC3, DNMT1, DNMT3A and DNMT3B Protein expressions in LV samples. Gap junctions, specialized plasma membrane domains composed of intercellular channel arrays, are vital for electrical and metabolic coupling between adjacent cardiomyocytes. Cx43 is the predominant gap junction protein in the ventricular myocardium. The present study revealed significant Cx43 downregulation in offspring exposed to maternal LPS compared with controls, with pronounced reductions observed at 8 weeks (P<0.01) and 16 weeks of age (P<0.01). This persistent Cx43 depletion suggests sustained gap junction impairment in the LV of prenatal LPS-exposed offspring. The present study further demonstrated dynamic alterations in cardiac autophagy. LC3 is a pivotal autophagy marker that exists in two isoforms: cytoplasmic LC3-I and autophagosome-associated LC3-II. At 8 weeks, prenatal LPS exposure resulted in significant suppression of autophagy activity as evidenced by a markedly decreased LC3II/I ratio (P<0.01) compared with controls. Conversely, this ratio was substantially elevated in 16-week-old LPS-exposed offspring (P<0.01), indicating the paradoxical activation of autophagy pathways at later developmental stages. Western blotting of LV tissues revealed a significant reduction in DNMT1 expression at 8 weeks (P<0.05), followed by pronounced upregulation at 16 weeks (P<0.01) compared with age-matched controls. Conversely, neither DNMT3A (P>0.05) nor DNMT3B (P>0.05) exhibited statistically significant differences between the experimental groups at either time point. Notably, while Cx43 exhibited discordance between protein and mRNA expression patterns, LC3 and DNMT1 demonstrated that the protein expression trends closely mirrored their respective mRNA levels (Fig. 5).

mRNA and protein expression of Cx43, LC3 and DNMT1 in rat primary cardiac fibroblasts. LPS stimulation was applied to rat primary CFs to establish a pathological model

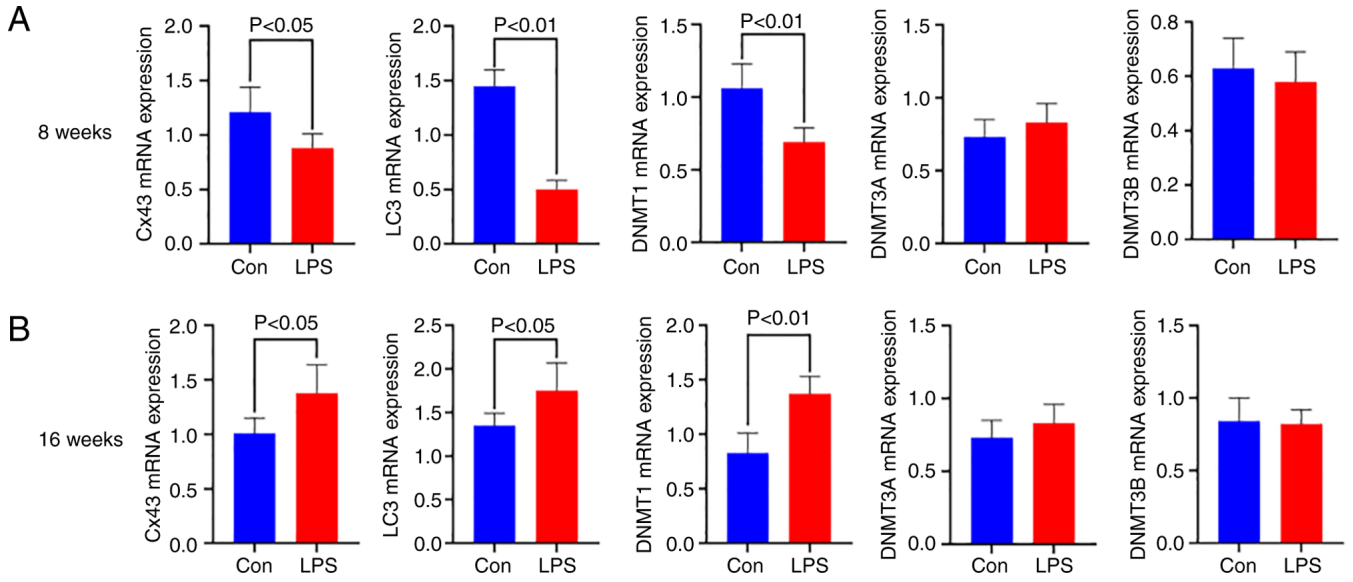

Figure 4. mRNA expression of Cx43, LC3, DNMT1, DNMT3A and DNMT3B in the LV from offspring rats at the age of (A) 8 and (B) 16 weeks. Data are presented as mean ± SD. n=6 in each group. Cx43, connexin 43; DNMT, DNA methyltransferase; LV, left ventricular; Con, control; LPS, lipopolysaccharide.

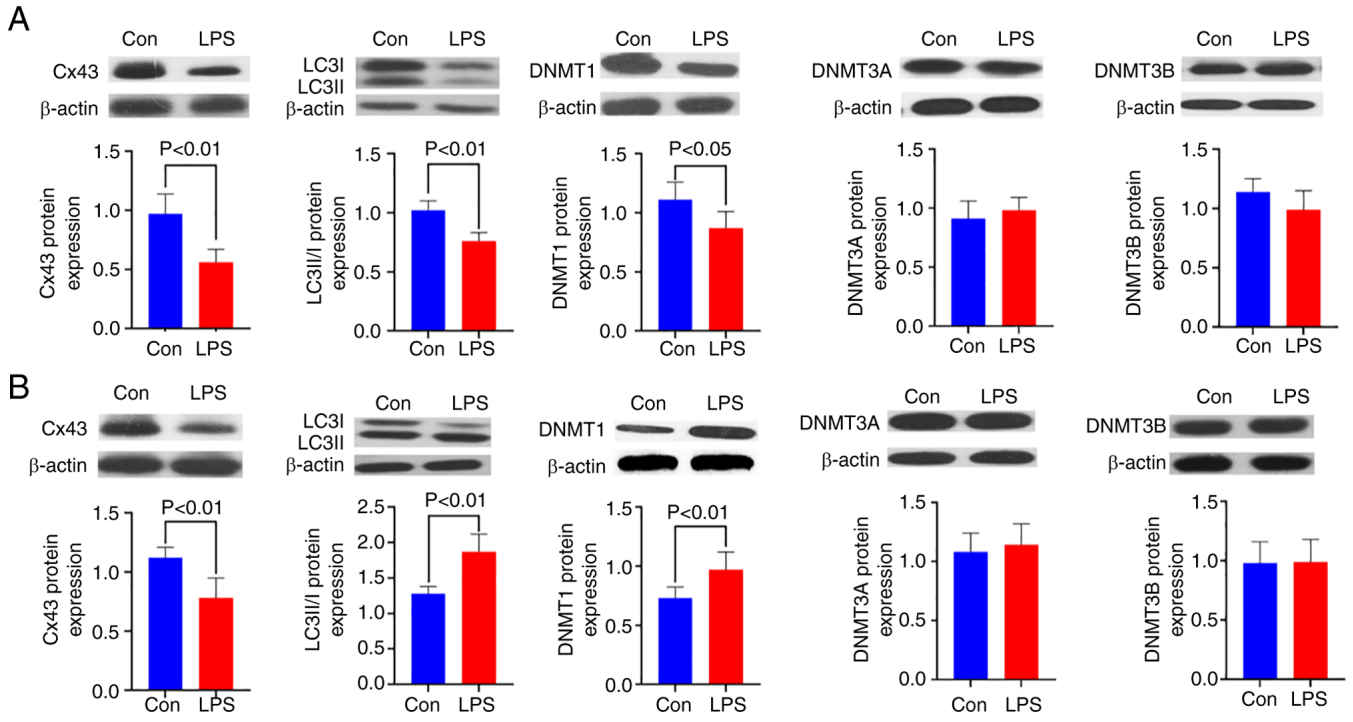

Figure 5. Protein expression of Cx43, LC3II/I, DNMT1, DNMT3A and DNMT3B in LV from offspring rat at (A) 8 and (B) 16 weeks. n=6 in each group. Cx43, connexin 43; DNMT, DNA methyltransferase; LV, left ventricular; Con, control; LPS, lipopolysaccharide.

mimicking the *in vivo* conditions observed in prenatal LPS-exposed offspring. Following 24 h LPS stimulation, both mRNA and protein levels of Cx43 and LC3 markedly down-regulated (P<0.01), whereas DNMT1 exhibited a pronounced up-regulation at the transcriptional and translational levels (P<0.05) compared with untreated controls. This molecular profile resembled the pathological changes observed in prenatal LPS-exposed offspring aged 8-16 weeks, establishing an *in vitro* model that recapitulates the key molecular features of developmental cardiac remodeling. To investigate Cx43-dependent mechanisms, Cx43 was pharmacologically modulated using CBX as an inhibitor and ATRA as an agonist. CBX treatment effectively suppressed Cx43 expression (P<0.05) and further reduced LC3 levels at the mRNA (P<0.01) and protein (P<0.05) levels, while also markedly attenuating DNMT1 expression (P<0.05 or 0.01) compared with LPS treatment alone. Cotreatment with LPS and ATRA increased both mRNA (P<0.05) and protein (P<0.05) expression of Cx43 compared with the LPS-stimulated group alone, subsequently restoring the protein and mRNA expression

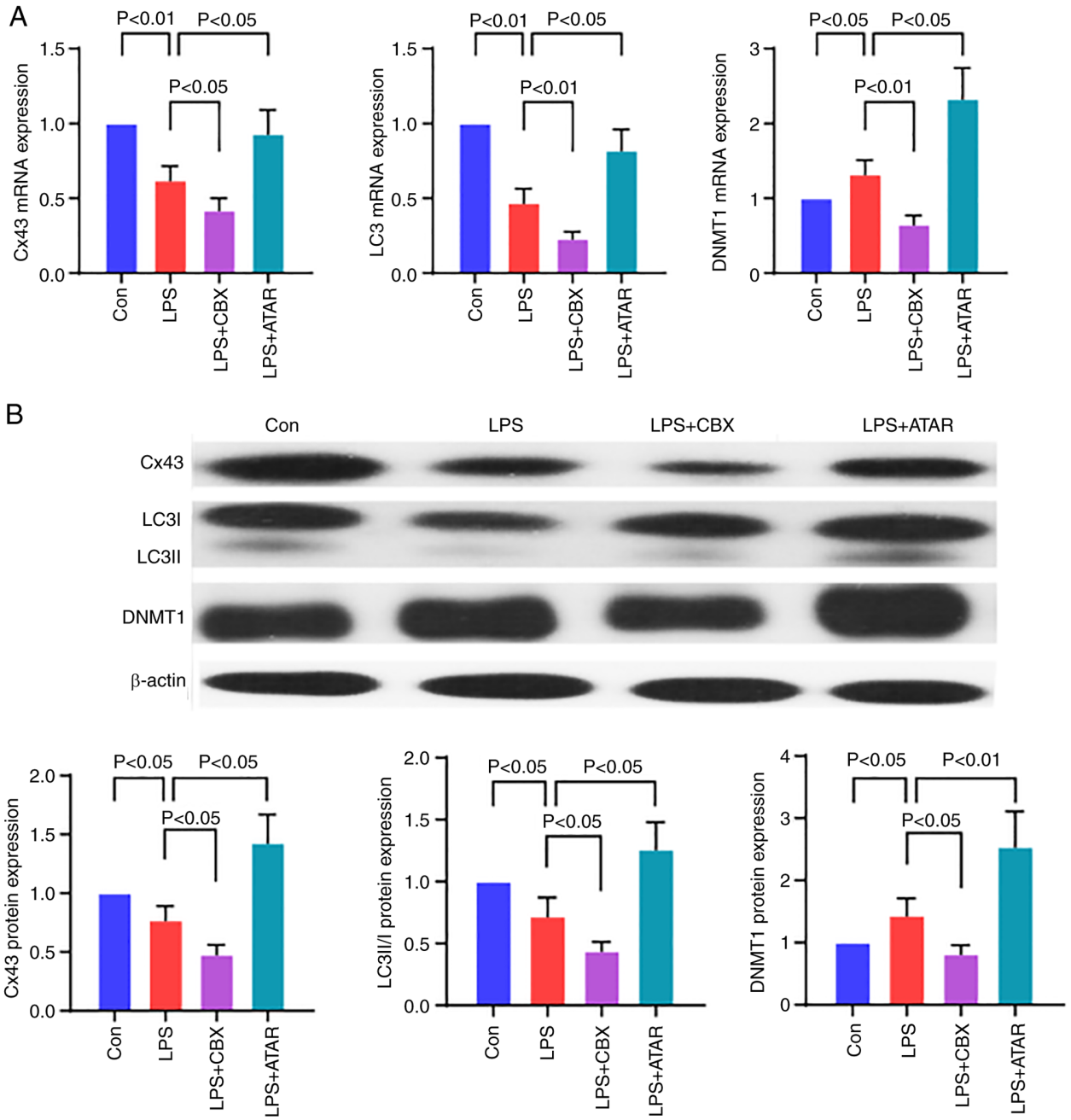

Figure 6. Effect of Cx43 on the expression of LC3 and DNMT1 *in vitro*. (A) mRNA and (B) protein expression of Cx43, LC3 and DNMT1 in rat primary cardiac fibroblasts. Data are presented as mean ± SD. n=3/group. Control group, rat primary cardiac fibroblasts treated with culture media; LPS group, rat primary cardiac fibroblasts treated with culture media containing 10 μg/ml LPS; LPS + CBX group, rat primary cardiac fibroblasts treated with culture media containing 10 μg/ml LPS and 400 μM CBX; LPS + ATRA group, rat primary cardiac fibroblasts treated with culture media containing 10 μg/ml LPS and 10 μM all-trans retinoic acid. Cx43, connexin 43; DNMT, DNA methyltransferase; LPS, lipopolysaccharide; CBX, carbenoxolone; ATRA, all-trans retinoic acid; Con, control; LPS, lipopolysaccharide.

levels of DNMT1 and LC3 (P<0.05 or 0.01). These results demonstrated that Cx43 regulates autophagy-related LC3 dynamics and DNMT1-mediated epigenetic modifications during fibrotic progression, reinforcing its position as an upstream node in this regulatory network (Fig. 6).

Discussion

The present study highlighted that maternal LPS exposure during pregnancy may induce a cardiac fibrotic shift. Notably, its key novel finding revealed age-dependent progressive fibrotic alterations in the hearts of prenatally LPS-exposed offspring rats, concomitant with reduced Cx43 expression. This extends our previous observations (3-5,18). Cx43, the predominant membrane protein forming ventricular GJs, is essential for maintaining cardiac electrophysiological homeostasis. Substantial evidence suggests that reduced Cx43 expression can trigger excessive collagen deposition in aged and pathologically remodeled hearts (7). Notably, pharmacological interventions targeting fibrotic pathways, including renin-angiotensin-aldosterone system inhibitors or TGF-β receptor blockers, ameliorate cardiac fibrosis

while restoring Cx43 expression. Similarly, GJ modifiers that upregulate Cx43 exhibit anti-fibrotic effects, even in the contexts of TGF-β pathway activation or pre-existing cardiovascular pathologies (19,20). Although the mechanistic association between Cx43 dysregulation and fibrosis remains incompletely understood, emerging studies have proposed that Cx43 deficiency may disrupt cardiomyocyte-fibroblast and fibroblast-fibroblast coupling, thereby promoting fibroblast activation, proinflammatory responses and collagen overproduction (7). Mechanistically, Cx43 downregulation via hemichannel blockade or autophagy-dependent degradation activates the MAPK/ERK pathway, which synergizes with Smad signaling to enhance collagen transcription and stabilize Col1a1 mRNA (21). Our prior study demonstrated persistent MAPK activation in the heart of LPS-exposed offspring rats, particularly when challenged with secondary stressors in adulthood (3). Furthermore, Cx43 facilitates microtubule-dependent trafficking of voltage-gated sodium channels (Nav1.5) to intercalated discs, suggesting its critical role in regulating Nav1.5 membrane localization and function. Therefore, Cx43 downregulation may impair Nav1.5 distribution, contributing to fibrosis via channel-independent mechanisms (22). Consistent with these findings, the present study revealed that Cx43 mediated GJ disruption and elevated α-SMA expression in the cardiac tissues of prenatally LPS-exposed offspring. Collectively, the present study proposed a novel paradigm in which intrauterine Cx43 suppression orchestrates ventricular fibrosis via channel-dependent and independent pathways, providing new insights into fibrotic pathogenesis. A key finding of the present study is that maternal LPS exposure induced localized, not systemic, RAS activation in the offspring heart, which is in line with previous observations (18,23). This localized activation is key, as Ang-II, the primary effector peptide of the RAS-has been demonstrated in a rat isolated perfused beating atrial model to directly downregulate Cx43 expression and to induce atrial fibrosis (24,25). Our previous studies further demonstrated that maternal LPS exposure during gestation induces offspring cardiac abnormalities, including localized inflammation, RAS activation, TGF-β upregulation and hemodynamic overload, all of which are potential contributors to Cx43 downregulation and GJ impairment (4,26). Consequently, Cx43 reduction is a consequence of adverse fetal programming and an active regulator of fibrotic progression.

Notably, while prenatal LPS exposure induced upregulated Cx43 mRNA expression in 16-week-old offspring rats, its protein levels were paradoxically decreased, suggesting post-translational Cx43 degradation. This observation aligns with the established role of autophagy in mediating protein turnover, which is particularly prominent under pathological stress (10). Consistent with this, there was a markedly elevated LC3-II/I ratio, a biomarker of autophagic flux, in 16-week-old LPS-exposed offspring, indicating that Cx43 downregulation may result from hyperactivated autophagy. In contrast to the 16-week cohort, 8-week-old LPS-exposed offspring exhibited suppressed LC3-II/I ratios. This temporal divergence suggests that autophagy may exert pleiotropic effects beyond Cx43 degradation in the present model. Functionally, autophagy is a lysosome-dependent quality control system that eliminates damaged cytoplasmic components, thereby maintaining homeostasis. Dysregulation of this process, whether insufficient or excessive, disrupts the myocardial protein/organelle balance, with autophagy deficiency leading to toxic aggregate accumulation and hyperactivation resulting in destructive self-digestion.

The relationship between autophagy and cardiac fibrosis is still unclear. For instance, transverse aortic constriction in mice for 8 weeks increased LV autophagy concomitantly with fibrosis progression (27). Similarly, renovascular hypertension induced myocardial autophagy specifically in domestic pigs with moderate but not mild hypertension and autophagic activity associated positively with fibrosis severity (28). Curcumin inhibited autophagy and attenuated isoproterenol-induced fibrosis in rodent models (9). However, endothelial-specific autophagy suppression, either by a specific inhibitor or siRNA for ATG5, exacerbates fibrotic responses *in vitro* and *in vivo* (29). These apparent contradictions likely stem from context-dependent variables, including disease etiology, stage and intervention timing. In the present experimental paradigm, prenatal inflammation primes offspring rats for autophagy-induced cardiac fibrosis. Notably, besides direct profibrotic effects, autophagy may indirectly perpetuate fibrosis via Cx43 dysregulation, thereby establishing a self-reinforcing loop.

The present study revealed dynamic changes in DNMT1 expression patterns in offspring rats exposed to prenatal LPS. The mRNA and protein levels of DNMT1 in cardiac tissue exhibited an initial decline at 8 weeks of age, followed by a rebound at 16 weeks. Conversely, DNMT3A and DNMT3B expression remained stable across these developmental stages. These temporal variations in DNMT1 activity may be key for cardiac fibrosis progression, given that CpG hypomethylation is implicated in fibrogenic genes transcriptional activation. This aligns with previous findings demonstrating that DNMT1 suppression in TGF-β-stimulated cardiac fibroblasts promotes α-SMA overexpression (30). Decreased DNMT1 levels enhance TGF-β receptor I expression, exacerbating fibroblast differentiation and fibrogenesis (30,31). Conversely, anti-fibrotic genes hypermethylation mediated by DNMT3B upregulation, as observed in SUN2 gene silencing during hepatic fibrosis (32), highlights the complex epigenetic regulation of fibrosis. Notably, the concurrent dysregulation of α-SMA, TGF-β and DNMT1 in the present model suggested a potential mechanistic link to Cx43 modulation.

The present study observed discordant temporal patterns between autophagy activity and DNA methylation dynamics during age-dependent fibrosis progression. This paradoxical relationship may reflect compensatory mechanisms that preserve cardiac homeostasis in younger offspring, consistent with prior reports that cardiac dysfunction in this model only manifests at 8 months of age (4). The present findings further implied both impaired autophagy and aberrant methylation patterns in Cx43 downregulation, highlighting their synergistic roles in modulating cellular responses during fibrotic remodeling. Emerging evidence positions Cx43 as a molecular nexus integrating diverse signaling pathways, suggesting that its interaction with epigenetic and autophagic regulators may operates through interconnected networks rather than isolated pathways (33). To clarify these interactions, the present

study used an *in vitro* LPS-treated cardiac fibroblast model with pharmacological interventions using a Cx43 inhibitor (CBX) and a Cx43 agonist (ATRA) (34,35), providing direct evidence of the central regulatory role of Cx43 in coordinating DNMT1 expression and autophagic activity. Cx43 inhibition blunted the LPS-triggered rise in DNMT1 but deepened the suppression of LC3, whereas its activation rescued the expression of both molecules. This dual effect aligns with the two established mechanisms of Cx43 function. First, by serving as an ATP-release channel that activates P2X7 purinergic receptors, Cx43 promotes autophagy induction through multiple signaling cascades, a process mechanistically associated with pressure overload-induced cardiac hypertrophy (36-38). Second, the Cx43 downregulation observed following prenatal inflammation engages MAPK signaling pathways, considering that pharmacological inhibition of MAPK restores DNMT1 expression in hypoxic cardiac progenitor cells (3,39). Collectively, these bidirectional manipulations confirm that Cx43 functions as an upstream modulator, whose activity state dynamically influences DNMT1-mediated epigenetic and autophagic responses in cardiac fibroblasts under inflammatory stress.

Furthermore, the observed cardiac DNMT1 biphasic, age-dependent regulation *in vivo,* characterized by suppression at 8 weeks followed by upregulation at 16 weeks, contrasts with its acute upregulation in LPS-stimulated cardiac fibroblasts *in vitro*. This apparent discrepancy likely originates from the fundamental differences in the experimental context, timeframe and biological complexity between the two models, which is a recognized challenge in translating *in vitro* findings to developmental programming phenotypes (40). *In vivo* findings reflect a chronic developmental programming process initiated by transient prenatal LPS exposure (41). Early DNMT1 downregulation may represent an initial, maladaptive, or compensatory response in the complex cardiac milieu, potentially facilitating the early expression of fibrogenic genes. Its subsequent rebound at 16 weeks could help stabilize the fibrotic phenotype or silencing protective pathways during later-stage remodeling. Conversely, the *in vitro* model captures the acute cellular response of isolated fibroblasts to direct and sustained LPS stimulation, which mimics immediate profibrotic activation and is marked by rapid DNMT1 induction (42). While this model recapitulates the key molecular features of fibroblast activation, it does not include the longer-term temporal evolution or multicellular interactions inherent to the *in vivo* programmed phenotype. Therefore, these two models are complementary. The *in vitro* system elucidates the acute cell-autonomous response, whereas the *in vivo* model reveals the integrated stage-specific epigenetic dynamics within the programmed heart.

The present study focused on elucidating the consequences of maternal LPS exposure during gestation on offspring cardiac fibrosis, revealing a significant association with aberrant Cx43 expression patterns. While its findings established a functional regulatory role for Cx43 activity, the precise mechanistic relationships underlying its interaction with autophagy and DNMT1-mediated epigenetic modifications warrant further investigation. The complex regulatory landscape of Cx43, including its hemichannel activity, phosphorylation status and subcellular localization, must be systematically dissected to understand how these specific facets differentially influence the fibrotic process under inflammatory stress. Future studies using genetic tools and pathway-specific inhibitors are crucial to map the exact downstream signaling cascades (for example, MAPK/ERK) that transduce Cx43 activity into alterations in autophagic flux and DNA methylation patterns.

Taken together, the data of the present study integrated with existing literature propose that Cx43 deficiency may serve as a molecular nexus connecting prenatal inflammatory insults to the developmental programming of cardiac fibrosis. This regulatory axis orchestrates a dynamic interplay between autophagic flux and DNA methylation machinery, potentially establishing persistent epigenetic imprints during cardiogenesis. These insights advance a novel paradigm for understanding fibrosis pathogenesis, in which early-life inflammatory challenges may prime the cardiac epigenome via Cx43-mediated pathways. Consequently, targeted interventions aimed at preserving Cx43 homeostasis during gestation could emerge as preventive strategies against adult-onset cardiovascular diseases by disrupting this developmental programming cascade.

Acknowledgements

Not applicable.

Funding

The present study was supported by grants from the National Natural Science Foundation of China (grant no. 81573440) and the Natural Science Foundation of Chongqing, China (grant no. cstc2019jcyj-msxmX0609).

Availability of data and materials

The data and materials in the current study are available from the corresponding author on reasonable request.

Authors' contributions

YL, YW and HGZ conceived and designed the research. YW performed experiments. YW and YY analyzed data. YL, YW and YY interpreted results of experiments. YL acquired funding. YW, YL and HGZ confirm the authenticity of all the raw data. YW and YY prepared figures. YW, YL and HGZ drafted the manuscript and YL edited and revised the manuscript. All authors read and approved the final manuscript.

Ethics approval and consent to participate

The present study complied with the Guide for the Care and Use of Laboratory Animals published by the US National Institutes of Health (NIH Publication N.85-23, revised 1996; http://www.nap.edu/readingroom/books/labrats/index.html) and received ethical approval from the Army Medical University Animal Care Committee (approval no. AMUWEC2020980).

Patient consent for publication

Not applicable.

Competing Interests

The authors declare that they have no competing interests.

References

1. Frangogiannis NG: Cardiac fibrosis. Cardiovasc Res 117: 1450-1488, 2021.
2. Barker DJP: The origins of the developmental origins theory. J Intern Med 261: 412-417, 2007.
3. Zhang Q, Deng Y, Lai W, Guan X, Sun X, Han Q, Wang F, Pan X, Ji Y, Luo H, *et al*: Maternal inflammation activated ROS-p38 MAPK predisposes offspring to heart damages caused by isoproterenol via augmenting ROS generation. Sci Rep 6: 30146, 2016.
4. Wei Y, Du W, Xiong X, He X, Yi P, Deng Y, Chen D and Li X: Prenatal exposure to lipopolysaccharide results in myocardial remodelling in adult murine offspring. J Inflamm (Lond) 10: 35, 2013.
5. Cao D, Liu Y, Chen X, Liu J, Liu J, Lai W, Li S, Wang W, Zhang W, Xiao D, *et al*: Activation of iNKT cells at the maternal-fetal interface predisposes offspring to cardiac injury. Circulation 145: 1032-1035, 2022.
6. Trovato-Salinaro A, Trovato-Salinaro E, Failla M, Mastruzzo C, Tomaselli V, Gili E, Crimi N, Condorelli DF and Vancheri C: Altered intercellular communication in lung fibroblast cultures from patients with idiopathic pulmonary fibrosis. Respir Res 7: 122, 2006.
7. Jansen JA, van Veen TAB, de Jong S, van der Nagel R, van Stuijvenberg L, Driessen H, Labzowski R, Oefner CM, Bosch AA, Nguyen TQ, *et al*: Reduced Cx43 expression triggers increased fibrosis due to enhanced fibroblast activity. Circ Arrhythm Electrophysiol 5: 380-390, 2012.
8. Cao L, Chen Y, Lu L, Liu Y, Wang Y, Fan J and Yin Y: Angiotensin II upregulates fibroblast-myofibroblast transition through Cx43-dependent CaMKII and TGF-β1 signaling in neonatal rat cardiac fibroblasts. Acta Biochim Biophys Sin (Shanghai) 50: 843-852, 2018.
9. Liu R, Zhang HB, Yang J, Wang JR, Liu JX and Lim CL: Curcumin alleviates isoproterenol-induced cardiac hypertrophy and fibrosis through inhibition of autophagy and activation of mTOR. Eur Rev Med Pharmacol Sci 22: 7500-7508, 2018.
10. Martins-Marques T, Catarino S, Zuzarte M, Marques C, Matafome P, Pereira P and Girão H: Ischaemia-induced autophagy leads to degradation of gap junction protein connexin43 in cardiomyocytes. Biochem J 467: 231-245, 2015.
11. Wang J, Cui J, Chen R, Deng Y, Liao X, Wei Y, Li X, Su M, Yu J and Yi P: Prenatal exposure to lipopolysaccharide alters renal DNA methyltransferase expression in rat offspring. PLoS One 12: e0169206, 2017.
12. Guan X, Dan GR, Yang Y, Ji Y, Lai WJ, Wang FJ, Meng M, Mo BH, Huang P, You TT, *et al*: Prenatal inflammation exposure-programmed hypertension exhibits multi-generational inheritance via disrupting DNA methylome. Acta Pharmacol Sin 43: 1419-1429, 2022.
13. Mohamed AS, Hosney M, Bassiony H, Hassanein SS, Soliman AM, Fahmy SR and Gaafar K: Sodium pentobarbital dosages for exsanguination affect biochemical, molecular and histological measurements in rats. Sci Rep 10: 378, 2020.
14. Fish RE, Brown MJ, Danneman PJ and Karas AZ: Anesthesia and analgesia in laboratory animals, 2nd edition. London: Elsevier, 2008.
15. Livak KJ and Schmittgen TD: Analysis of relative gene expression data using real-time quantitative PCR and the 2(-Delta Delta C(T)) method. Methods 25: 402-408, 2001.
16. Kelishadi R, Haghdoost AA, Jamshidi F, Aliramezany M and Moosazadeh M: Low birthweight or rapid catch-up growth: which is more associated with cardiovascular disease and its risk factors in later life? A systematic review and cryptanalysis. Paediatr Int Child Health 35: 110-123, 2015.
17. Cao Z, Jia Y and Zhu B: BNP and NT-proBNP as diagnostic biomarkers for cardiac dysfunction in both clinical and forensic medicine. Int J Mol Sci 20: 1820, 2019.
18. Hao XQ, Zhang HG, Yuan ZB, Yang DL, Hao LY and Li XH: Prenatal exposure to lipopolysaccharide alters the intrarenal renin-angiotensin system and renal damage in offspring rats. Hypertens Res 33: 76-82, 2010.
19. Patin J, Castro C, Steenman M, Hivonnait A, Carcouët A, Tessier A, Lebreton J, Bihouée A, Donnart A, Le Marec H, *et al*: Gap-134, a Connexin43 activator, prevents age-related development of ventricular fibrosis in $Scn5a^{+/-}$ mice. Pharmacol Res 159: 104922, 2020.
20. Stein M, Boulaksil M, Jansen JA, Herold E, Noorman M, Joles JA, van Veen TAB, Houtman MJC, Engelen MA, Hauer RNW, *et al*: Reduction of fibrosis-related arrhythmias by chronic renin-angiotensin-aldosterone system inhibitors in an aged mouse model. Am J Physiol Heart Circ Physiol 299: H310-H321, 2010.
21. Wu L, Wang Z, He X, Jiang Y, Pan R, Chen S, Chen Y, Han Y, Yu H and Zhang T: GJA1 reverses arsenic-induced EMT via modulating MAPK/ERK signaling pathway. Toxicol Appl Pharmacol 450: 116138, 2022.
22. Jansen JA, Noorman M, Musa H, Stein M, de Jong S, van der Nagel R, Hund TJ, Mohler PJ, Vos MA, van Veen TA, *et al*: Reduced heterogeneous expression of Cx43 results in decreased Nav1.5 expression and reduced sodium current that accounts for arrhythmia vulnerability in conditional Cx43 knockout mice. Heart Rhythm 9, 600-607, 2012.
23. Gao M, Zhang X, Chen X, Mi C, Tang Y, Zhou J and Li X: Prenatal exposure to lipopolysaccharide results in local RAS activation in the adipose tissue of rat offspring. PLoS One 9: e111376, 2014.
24. Ding DZ, Jia YN, Zhang B, Guan CM, Zhou S, Li X and Cui X: C-type natriuretic peptide prevents angiotensin II-induced atrial connexin 40 and 43 dysregulation by activating AMP-activated kinase signaling. Mol Med Rep 20: 5091-5099, 2019.
25. Li X, Cui X, Zhou S, Xing DL, Piao HR, Zhang QG, Zhao YQ and Liu LP: The novel ginsenoside AD2 prevents angiotensin II-induced connexin 40 and connexin 43 dysregulation by activating AMP kinase signaling in perfused beating rat atria. Chem Biol Interact 339: 109430, 2021.
26. Chen X, Tang Y, Gao M, Qin S, Zhou J and Li X: Prenatal exposure to lipopolysaccharide results in myocardial fibrosis in rat offspring. Int J Mol Sci 16: 10986-10996, 2015.
27. Zhang Y, Wang Z, Lan D, Zhao J, Wang L, Shao X, Wang D, Wu K, Sun M, Huang X, *et al*: MicroRNA-24-3p alleviates cardiac fibrosis by suppressing cardiac fibroblasts mitophagy via downregulating PHB2. Pharmacol Res 177: 106124, 2022.
28. Zhang X, Gibson ME, Li ZL, Zhu XY, Jordan KL, Lerman A and Lerman LO: Autophagy portends the level of cardiac hypertrophy in experimental hypertensive swine model. Am J Hypertens 29: 81-89, 2016.
29. Pan JA, Zhang H, Lin H, Gao L, Zhang HL, Zhang JF, Wang CQ and Gu J: Irisin ameliorates doxorubicin-induced cardiac perivascular fibrosis through inhibiting endothelial-to-mesenchymal transition by regulating ROS accumulation and autophagy disorder in endothelial cells. Redox Biol 46: 102120, 2021.
30. He Y, Ling S, Sun Y, Sheng Z, Chen Z, Pan X and Ma G: DNA methylation regulates α-smooth muscle actin expression during cardiac fibroblast differentiation. J Cell Physiol 234: 7174-7185, 2019.
31. Fu S, Sun L, Zhang X, Shi H, Xu K, Xiao Y and Ye W: 5-Aza-2'-deoxycytidine induces human Tenon's capsule fibroblasts differentiation and fibrosis by up-regulating TGF-β type I receptor. Exp Eye Res 165: 47-58, 2017.
32. Chen X, Li WX, Chen Y, Li XF, Li HD, Huang HM, Bu FT, Pan XY, Yang Y, Huang C, *et al*: Suppression of SUN2 by DNA methylation is associated with HSCs activation and hepatic fibrosis. Cell Death Dis 9: 1021, 2018.
33. Fournier S, Clarhaut J, Cronier L and Monvoisin A: GJA1-20k, a short isoform of Connexin43, from its discovery to its potential implication in cancer progression. Cells 14: 180, 2025.
34. Miura M, Nagano T, Murai N, Taguchi Y, Handoh T, Satoh M, Miyata S, Miller L, Shindoh C and Stuyvers BD: Effect of carbenoxolone on arrhythmogenesis in rat ventricular muscle. Circ J 80: 76-84, 2016.
35. Liu Y, Wen Q, Chen XL, Yang SJ, Gao L, Gao L, Zhang C, Li JL, Xiang XX, Wan K, *et al*: All-trans retinoic acid arrests cell cycle in leukemic bone marrow stromal cells by increasing intercellular communication through connexin 43-mediated gap junction. J Hematol Oncol 8: 110, 2015.
36. Sun L, Gao J, Zhao M, Cui J, Li Y, Yang X, Jing X and Wu Z: A novel cognitive impairment mechanism that astrocytic p-connexin 43 promotes neuronic autophagy via activation of P2X7R and down-regulation of GLT-1 expression in the hippocampus following traumatic brain injury in rats. Behav Brain Res 291: 315-324, 2015.

37. Orioli E, De Marchi E, Giuliani AL and Adinolfi E: P2X7 receptor orchestrates multiple signalling pathways triggering inflammation, autophagy and metabolic/trophic responses. Curr Med Chem 24: 2261-2275, 2017.
38. Higashikuni Y, Liu W, Numata G, Tanaka K, Fukuda D, Tanaka Y, Hirata Y, Imamura T, Takimoto E, Komuro I and Sata M: NLRP3 inflammasome activation through heart-brain interaction initiates cardiac inflammation and hypertrophy during pressure overload. Circulation 147: 338-355, 2023.
39. Su J, Fang M, Tian B, Luo J, Jin C, Wang X, Ning Z and Li X: Hypoxia induces hypomethylation of the HMGB1 promoter via the MAPK/DNMT1/HMGB1 pathway in cardiac progenitor cells. Acta Biochim Biophys Sin (Shanghai) 50: 1121-1130, 2018.
40. Lynch F, Lewis S, Macciocca I and Craig JM: Epigenetics and DOHaD: How translation to predictive testing will require a better public understanding. J Dev Orig Health Dis 13: 424-430, 2022.
41. Deng Y, Song L, Nie X, Shou W and Li X: Prenatal inflammation exposure-programmed cardiovascular diseases and potential prevention. Pharmacol Ther 190: 159-172, 2018.
42. Liu Z, Gao L, Kan C, Chen X, Shi K and Wang W: DNMT1 methylation of LncRNA-ANRIL causes myocardial fibrosis pyroptosis by interfering with the NLRP3/Caspase-1 pathway. Cell Mol Biol (Noisy-le-grand) 70: 197-203, 2024.